Journal of Space Safety Engineering xxx (xxxx) xxx

Contents lists available at ScienceDirect

Journal of Space Safety Engineering

journal homepage: www.elsevier.com/locate/jsse

Investigation of material response to atmospheric re-entry exposure of sub-structural Ti-6Al-4V components recovered from Space Shuttle *Columbia*

N.C. Ubani Ochoa*, A.C. Smith, D.M. Cone, S.W. Stafford, J.D. Olivas

Center for the Advancement of Space Safety and Mission Assurance Research (CASSMAR), The University of Texas at El Paso (UTEP), 500W. University Ave, El Paso, TX 79968, United States

ARTICLE INFO

Keywords:
Titanium alloys
Ti-6Al-4V
Bulk-metal combustion
Atmospheric re-entry
Space Shuttle *Columbia*

Article history:
Received 26 September 2020
Accepted 14 December 2020
Available online xxx

ABSTRACT

Aluminum and titanium char-layer deposits discovered on overhead windows recovered from the Space Shuttle *Columbia* accident revealed unexpected material response. It was observed that titanium melted and deposited before aluminum: behavior inconsistent with their relative melting temperatures. In close proximity to the windows, payload bay door (PLBD) latch rollers, containing Ti-6Al-4V, exhibited significant thermal damage that could not be explained by re-entry heating alone. The roller was considered a likely source of the deposition as damage was localized to the titanium region and the component was evaluated to identify features of ignition and/or combustion. A second examination was conducted on arc-jet samples obtained from a previous work that studied Ti-6Al-4V combustibility in a simulated re-entry environment. The samples were compared to the analysis of the PLBD roller and both exhibited features suggestive of titanium combustion. The PLBD roller possessed microstructural similarities to the arc-jet specimens that reacted more aggressively to the simulated environment.

1. Introduction

Space Shuttle *Columbia* lifted off from the Kennedy Space Center on January 16, 2003, for a 16-day microgravity and Earth science research mission. During its descent on February 1, 2003, *Columbia* was destroyed and the seven crew members aboard lost their lives. Amongst post-accident investigations, analysis of charred deposits discovered on fragments of overhead crew module Window 7 and Window 8 revealed unprecedented material behavior. The deposition was multi-layered, characterized by an inner layer comprising of titanium dioxide, (TiO_2, rutile), a layer containing TiO_2 grains with an aluminosilicate phase, and an outer porous layer of a 2000-series aluminum alloy [1]. Given the relative difference in melting temperatures, the unexpected behavior of titanium depositing prior to aluminum prompted study into the possible mechanisms responsible for the event. Examination of shuttle debris in close nominal proximity to the overhead windows, revealed severe thermal degradation, particularly to titanium-containing components, such as the payload bay door (PLBD) latch rollers, of which this paper takes focus. It was observed that in the immediate vicinity of the thermally affected titanium of the PLBD roller, lower melting alloy systems sustained significantly less damage suggesting material selectivity of the erosion. It was further determined that re-entry heating was an unlikely cause of the highly localized thermal damage and other heating mechanisms were considered [2,1].

An accelerated oxidative reaction was explored as a possible thermal mechanism and serves as the primary focus of the present investigation. Bulk titanium combustion, the reaction subsequent to exothermic oxide formation involves exponential temperature excursion of the metal, typically accompanied with metal surface boiling and ejection of molten particles. Titanium and titanium alloys are utilized in several aerospace applications for their excellent mechanical properties at elevated temperatures, the research and experimentation of which has been exhaustive. However, titanium has demonstrated extreme reactivity in the presence of oxygen, presenting a risk for its use, yet the subject has not been thoroughly explored to fully understand reaction mechanisms and establish predictability for design consideration.

Subsequent to the post-accident findings, Olivas, et al. launched a test program at the Boeing St. Louis Large Core Arc Tunnel plasma arc facility to investigate ignition and combustion behavior of titanium alloy Ti-6Al-4V in simulated high-enthalpy, low-pressure re-entry conditions predicted from the Space Shuttle *Columbia* accident. The results revealed that the Ti-6Al-4V samples ($7.6 \times 7.6 \times 0.25$-cm) exhibited reactive responses in certain enthalpy and heating rate conditions, which Olivas et al. characterized into three classifications: *Class I* - passivation; stable to quasi stable oxide layer growth. This layer, even after spalling and environmental exposure, re-develops the oxide layer that continues to protect the bulk material. *Class II* - ignition; environmental conditions initiate exothermic surface reactions that result in melting

* Corresponding author.
E-mail addresses: ncubani@miners.utep.edu (N.C.U. Ochoa), acsmith2@miners.utep.edu (A.C. Smith), dmcone@utep.edu (D.M. Cone), stafford@utep.edu (S.W. Stafford), jdo@oms117.com (J.D. Olivas).

https://doi.org/10.1016/j.jsse.2020.12.003
2468-8967/© 2020 Published by Elsevier Ltd on behalf of International Association for the Advancement of Space Safety.

Please cite this article as: N.C.U. Ochoa, A.C. Smith, D.M. Cone et al., Investigation of material response to atmospheric re-entry exposure of

Table 1
Table Alloy type and notation of each sleeve.

Position Number[a]	Alloy	Sleeve Notation
1	A-286	A286(A)
2	Chromium-plated IN718	CrIN718(B)
3	IN-718	IN718-C
4	IN-718	IN718-D
5	Ti-6Al-4V	Ti6Al4V(E)
6	Ti-6Al-4V	Ti6Al4V(F)
7	A-286	A286(G)
8	IN-718	IN718(H)

[a] Position 1 – outermost sleeve, Position 8 – innermost sleeve.

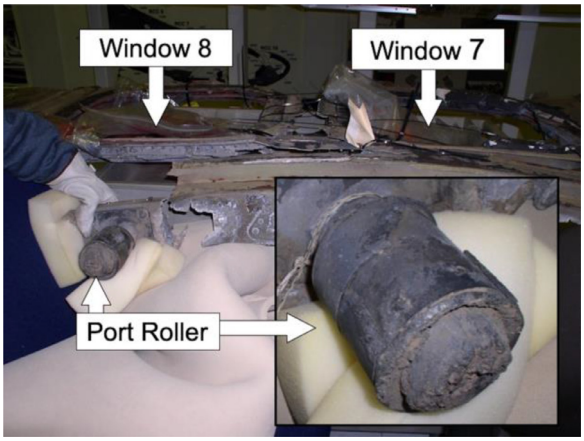

Fig. 1. (a) Debris components recovered Columbia (b) Close up view of PLBD port roller.

upon continued exposure. Evidence of oxide growth and reformation is observed although heating rates exceed the time necessary for stable oxide growth. *Class III* - ignition and combustion; exothermic reaction at the surface progresses at a rate such that stable oxide film growth is not possible.

The observed ignition and combustion behavior demonstrated a strong dependence upon sample geometry, as only samples with a 1.52-cm protuberance in the path of oxidizing flow exhibited a reaction. The role of geometry on ignition and combustion is not well understood, and further elicits the critical need for comprehensive study of the reaction mechanism in re-entry conditions if titanium alloys continue to find sub-structural application in space vehicles for which compromise of the thermal protection system may lead to loss of life [3].

The focus of this paper is the analysis of a forward PLBD latch roller component, located along the X_o582 ring-frame bulkhead of the orbiter, containing Ti-6Al-4V. The PLBD rollers serve as a part of the latch mechanism for securing the PLBDs of the midbody.

The PLBD roller construction is comprised of nine concentric sleeve-type components designed such that the sleeve components may each slide axially and telescope. Table 1 provides a sequential list of each sleeve alloy type and position label as confirmed by chemical analysis. Fig. 1 shows a recovered PLBD port-side roller in nominal arrangement with Window 7 and Window 8. A close-up view displays the deterioration of the port roller, illustrating localized damage to the titanium, which was also seen in other recovered PLBD rollers. This observation, along with the close proximity of the components to overhead windows, led investigators to name the PLBD rollers as a likely source of the window char deposition [2].

The current study also includes microstructural analysis of arc-jet samples in attempts to characterize the distinguishing microstructural features of each class and compare to the Ti-6Al-4V microstructure of the PLBD rollers. Microstructures of an untested, Class I, Class II and Class III sample were examined. Although the conditions in which the PLBD

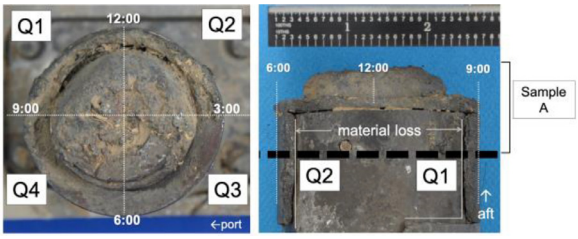

Fig. 2. Reaction front with clock face configuration and quadrants labeled (left) Sample A section outlined in black dashed line (right).

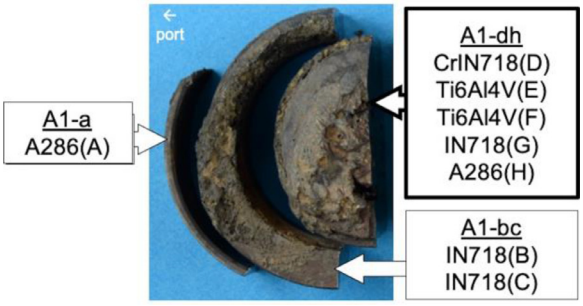

Fig. 3. Sample A1-dh containing Ti-6Al-4V sleeves outlined in bold.

rollers and the arc-jet samples reacted cannot be confidently related, and the arc-jet plate geometry is vastly different from the multi-alloy PLBD roller geometry and construction, there is still great value in the examination and comparison of titanium in actual and simulated re-entry environments.

2. Experimental methods

2.1. PLBD roller

Sample A was obtained by a transverse section made approximately 3.81-cm. from the thermally degraded base of the cylindrically-shaped roller, referred to as the reaction front. Provided in Fig. 2 is a forward-facing view of the reaction front with a clock face designation and quadrant delineation to identify reaction front surface regions, Q1-Q4. For surface characterization of the port roller, light optical microscopy (LOM) with a Keyence stereo microscope and scanning electron microscopy (SEM) with a Hitachi S-4800 microscope was employed. Fig. 3 contains sections of Sample A1, which is the isolation of Q1 and Q4 by an axial section of Sample A, made from 12:00 to 6:00. The sleeve(s) contained in each sub-sample is indicated in Fig. 4. This paper will only discuss the Ti-6Al-4V regions of Sample A1-dh.

Standard metallographic techniques were used for preparation of samples. The Ti-6Al-4V sleeves were selectively etched with Kroll's reagent (46-mL H_2O, 3-mL HNO_3, 1-mL HF). Microstructural analysis was performed, using LOM with an Olympus PME 3 inverted light optical microscope, on the axial cross-sections of the Ti-6Al-4V sleeves. Additional analysis includes SEM and backscatter scanning electron microscopy (BSE) using Hitachi S-4800 as well as an FEI XL30 scanning electron microscope.

2.2. Arc-jet test specimens

Test specimens, one from Class I, Class II, and Class III, and an untested control specimen, were sectioned axially for microstructural examination of the cross-section, as shown in Fig. 5. Samples were vacuum-impregnation mounted in an epoxy resin, prepared using standard metallographic techniques and etched with Kroll's reagent. The arc-jet plates were examined through their cross section with the arc-jet

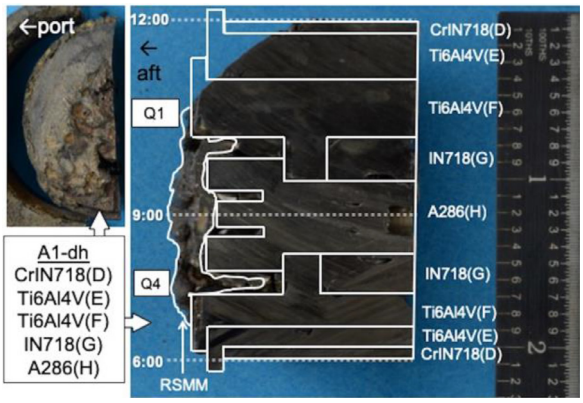

Fig. 4. Sample A1-dh: reaction front view (left) and axial cross-section (right) with sleeves outlined in white.

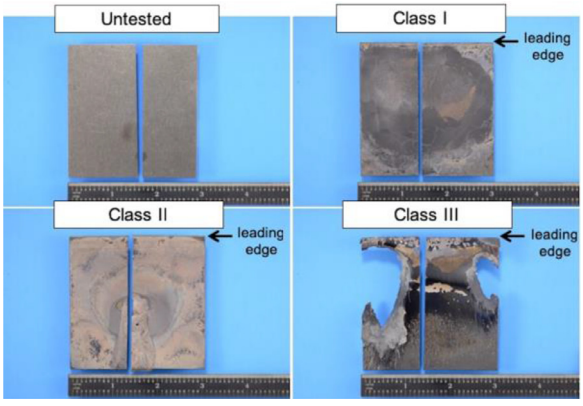

Fig. 5. Images of sectioned arc-jet samples.

flow facing the bottom of the image and the back side of the plate at the top of the images shown.

3. Results

3.1. PLBD roller surface analysis

The external surfaces of the port roller had a charred, dull appearance, with areas of discoloration and contamination, as shown in Fig. 6. The RSMM exhibited a slanting nature downward, with its steepest region seen in Q1 and Q2, Fig. 6b. This region coincided with the area where A286(A) experienced significant material loss. A close up of the RSMM can be seen in Fig. 6c. In contrast, little to no material loss was seen in Q3 as the area contained no evidence of significant melting. With higher magnification, several cavities (Figs. 6d-e) were resolved on the reaction front, one of which, contained a purple patina interior wall coating, shown in Fig. 6e.

Analysis of the reaction front using SEM also revealed varied surface features and textures. In the RSMM region of the reaction front, as well as in the degraded area of the outer sleeve, the surface contained a dimpled, porous texture (Fig. 7a). Throughout the entire sample, a globular morphology was observed (Fig. 7b) and the globules varied in size. Also observed in the thermally degraded area, was a ridged surface pattern, shown in Fig. 7c. On areas that exhibited little degradation, the surface exhibited mud-cracking, shown in Fig. 7d. Multilayered scales were also seen in several areas throughout the surface, (Fig. 7e-f).

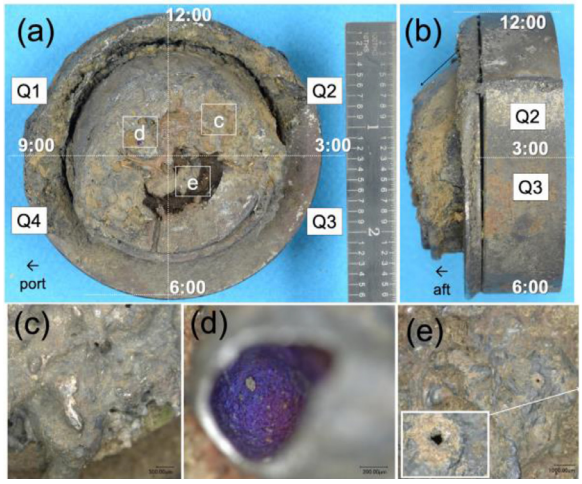

Fig. 6. Sample A (a) Reaction front (b) slanting RSMM of reaction front shown (c)-(e) magnified images of reaction front corresponding to white boxed regions outlined in 7a.

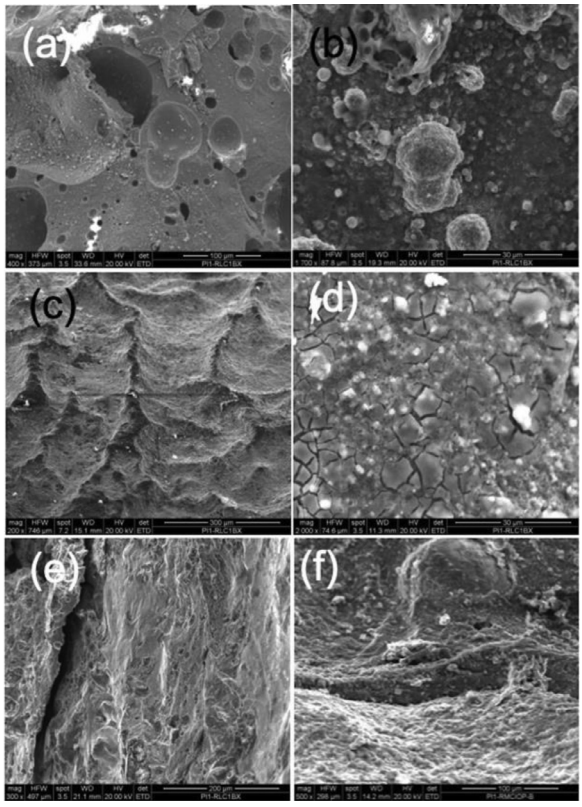

Fig. 7. SEM images of reaction front exhibiting varied surface texture: (a) spherical (b) porous oxide morphology, (c) Surface ridges (d) mud-cracked texture and (e)-(f) multi-layered scale formation.

3.2. PLBD roller microstructural analysis

3.2.1. PLBD roller – re-solidified molten material (RSMM)

The RSMM of the reaction front was observed both as surface deposition and as part of the bulk sleeve. Fig. 8 provides outlined regions from which micrographs in Figs. 9 –14 were obtained. As seen in Fig. 9a, the RSMM deposit on the outer diameter (OD) of Ti6Al4V(E)-Q1 contained a dendritic grain structure. The RSMM on Ti6Al4V(E)-Q1 is shown as part of the bulk and contained equiaxed grains and voids measuring over 0.1-mm in diameter (Fig. 9b).

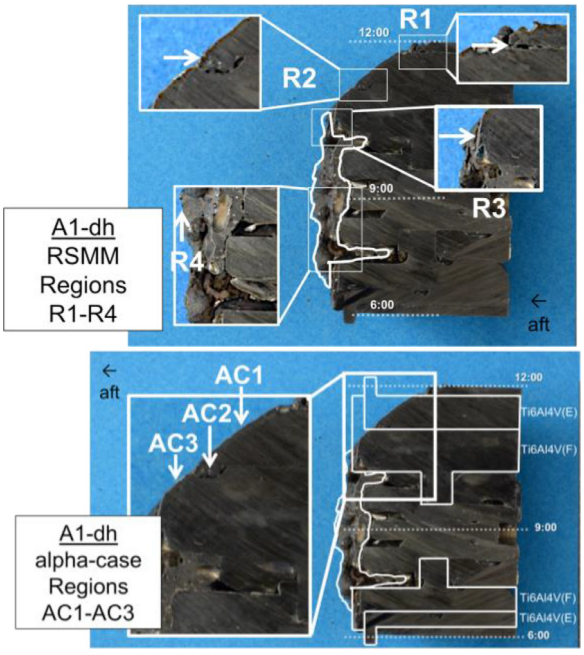

Fig. 8. Image of Sample A1-dh with Regions R1-R4 of RSMM and α-case layer Regions AC1-AC3 labeled and outlined in white at the bulk edge surfaces.

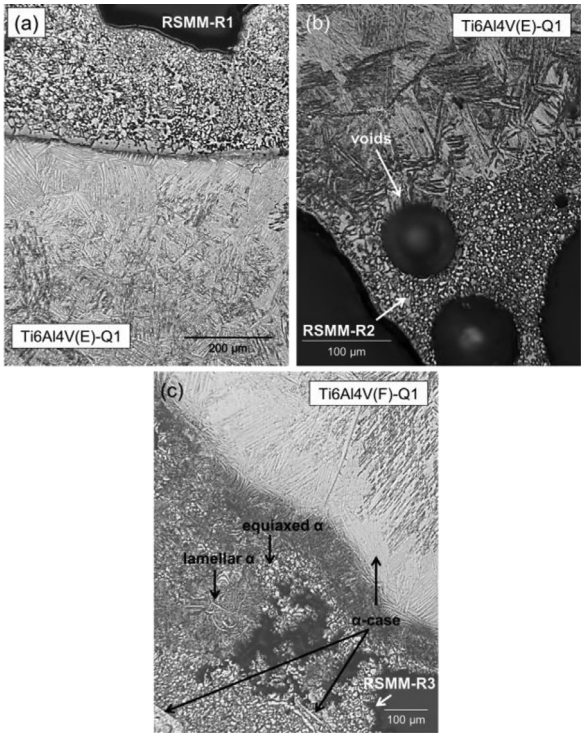

Fig. 9. (a) RSMM deposition on Ti6Al4V(E)-Q1, 100X (b) RSMM of Ti6Al4V(E), 200X (c) RSMM deposition/Ti6Al4V(F) interface, 100X; Kroll's.

The RSMM in Fig. 9c displayed shrinkage porosity and contained a mixed morphology of globular α and various regions of lamellar α in a β-phase matrix. The mixed morphology of the RSMM can also be viewed in Fig. 10b. The RSMM of the Q4 region contained spherical voids, measuring up to 0.3-mm in diameter (Fig. 10c), and the RSMM also exhibited irregular-shaped islands of lamellar α, Fig. 10c-d.

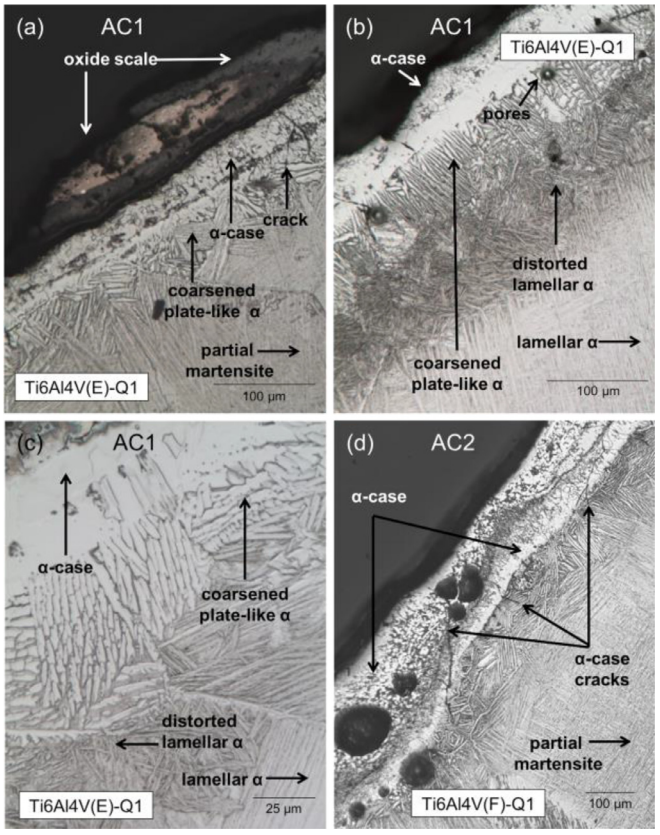

Fig. 10. RSMM deposition in Q1 (a) multi-layered α-case, 100X (b) α-case region with variable width, 500X (c) α-case stringers, 100X (d) distinct, uniform α-case layer, 100X; Kroll's.

3.2.2. PLBD roller – alpha-case and oxides

The oxygen-enriched α-case layer was observed throughout the reaction front region within the microstructure of the RSMM and along the bulk surface edges of Ti6Al4V(E) and Ti6Al4V(F). The morphology of α-case was varied throughout and measured from 15- to 25-μm in width. The presence of α-case is understood to form within the bulk of titanium alloys along with and adjacent to the formation of a surface oxide layer. Although the α-case observed in this investigation was not always present with a surface oxide scale, and often exhibited diverse features, it was clearly identified in micrographs as a distinct, light-colored region, which serves as an indication of increased α stabilization.

The α-case of the RSMM, can be seen in a multi-layered arrangement in Fig. 10a (layers measuring approximately 75-μm in thickness). The RSMM in Fig. 10b illustrates an α-case region of varied thickness, 15- to 25-μm in width, containing dark regions of β-phase within the coarsened globular α-case. Small, irregular-shaped oxygen-enriched stringers (Fig. 9c, Fig. 10a and c) were also present within the RSMM, measuring approximately 10- to 50-μm in width. In Fig. 10d, α-case formation is shown with an oxide scale present at the surface of the RSMM in Q4. The oxide was discontinuous and measured approximately 15-μm in width. The α-case layer beyond the oxide scale was uniform, (20-μm) with a smooth texture and non-descript grains, which represents a full stabilization of the α-phase.

Moving beyond the RSMM, the near-surface bulk contained varied morphology. Fig. 9a displays a near-edge bulk morphology characterized by a light region of coarsened lamellar α and a dark region of coarsened lamellar alpha can be seen in Fig. 9b. Fig. 11a provides a region of the Ti6Al4V(E)-Q1 bulk that contained a porous, mound-shaped oxide surface deposit, approximately 1-mm in length, and 75- and 10-μm in maximum and minimum thickness, respectively. This dark-colored oxide, with a light pink center, contained cracking and appeared to be

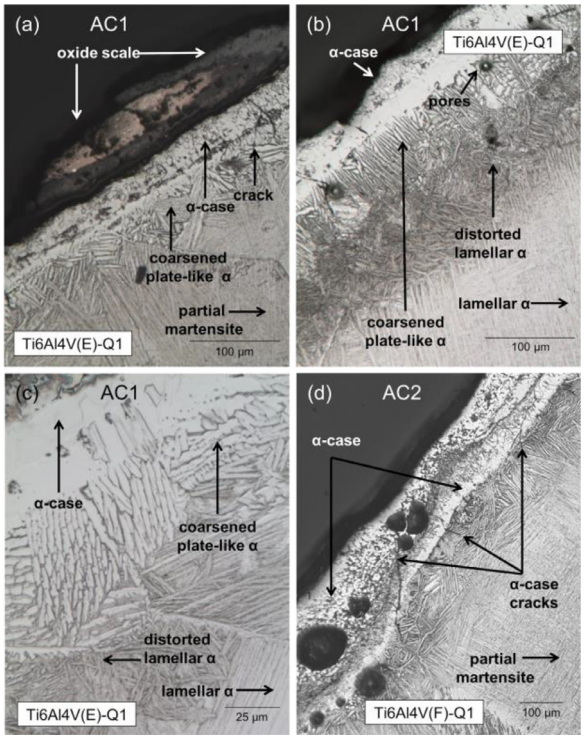

Fig. 11. Micrograph of α-case layers observed at the bulk edge surface of Ti6Al4V(E)-Q1 in (a)-(b) AC1, 200X, (c) 500X and (d) Region AC2, 100X; Kroll's.

weakly adherent to the surface. The corresponding α-case layer seen adjacent to the oxide deposit contained a thin ~1-μm linear region that appeared well-defined and etched dark, an indication of the β phase. This linear feature served to delineate two morphologies of the α-case layer: a globular morphology, measuring approximately 40-μm in uniform thickness, and a featureless morphology, containing solid α phase and extending 15-μm into the bulk. In a region where no surface oxide was resolved on the Ti6Al4V(E)-Q1 sleeve, globular α, with grain boundary β, characterized the α-case (15- to 30-μm in depth) adjacent to the jagged, rough surface (Fig. 11b-c). The α-case then transitioned into a uniform, featureless layer of solid white alpha (30-μm depth) in result of having a full-α structure.

Similar to the RSMM, Ti6Al4V(F)-Q1 also contained regions of multi-layered α-case formation, Fig. 11d, separated by a dark layer of fine, globular grains. With no adjacent surface oxide present, the outermost α-case was characterized by globular α (light) and β phase (dark) apparent at the grain boundaries. Containing less β phase, the inner α-case layer was more homogenous. Pores and cracks were prevalent throughout both α-case layers and the transitional region of coarse plate-like α that extends away from the α-case layer into the bulk, approximately 150-μm in depth, where the transition to a partial martensitic structure was observed.

The micrographs of Fig. 11 display a distinct transitional region beyond the α-case consisted of coarse, unidirectional, finger-like clusters of α phase that extended away from the α-case layer and measured approximately 50-μm in depth. Voids appeared localized to this region of transition. Moving into the bulk, a second transition was observed, where less coarse, plate-like α was present in a dark-colored woven arrangement of measuring 50- to 60-μm in depth, beyond the plate-like α. Beyond this point, a partial martensitic structure was apparent, defined by both, fine acicular α' and retained prior α lamellae, within prior β grains.

On OD surfaces at the reaction front (normal to the reaction plane) of the Ti6Al4V(E) and Ti6Al4V(F) sleeves in Q1, inner-sleeve spacing is increased due to a machined notch of the Ti6Al4V(F) sleeve. Here,

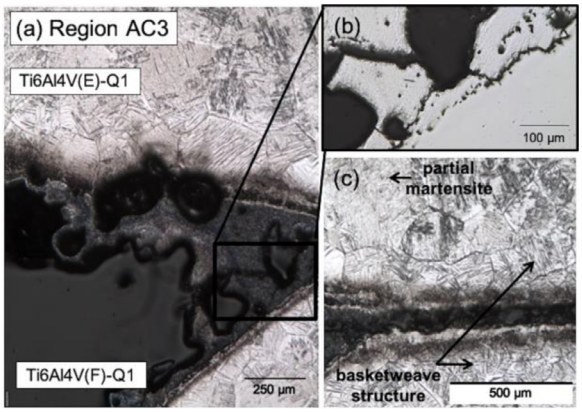

Fig. 12. Micrograph of inner sleeve OD (a) notch region, 150X (b) As-polished micrograph of (a), 150X; (c) beyond notch region, 100X; Kroll's.

deposition was observed and appeared sintered and oxidized, Fig. 12a. As seen in the as-polished micrograph in Fig. 12b, the oxide exhibited a shiny, rough texture. The micrograph of Fig. 12c shows deposition on the OD surfaces beyond the notch region, approximately 1.0-mm. The pores within the deposition on Ti6Al4V(E)-Q1 measured 5- to 250-μm in diameter, with coalesced voids seen partially within the bulk. The pores on Ti6Al4V(F)-Q1 were seen only within the deposition and measured smaller (5- to 25-μm in diameter). The α-case on the inner-sleeve OD surfaces of Ti6Al4V(E)-Q1 and Ti6Al4V(F)-Q1 measured approximately 30-μm and 60-μm in depth, respectively. In areas where voids were present within the bulk, a distinct α-case layer was not observed.

A linear region of dark discoloration, approximately 15-μm in thickness, was observed within the α-case layers in the notch region which, as seen in as-polished micrograph of Fig. 12b, contained coalesced voids that compromised adherence of the scale to the Ti6Al4V(F) surface. In contrast, no voids or crack-like features were evident corresponding to the dark delineated region in the α-case layer of the Ti6Al4V(E)-Q1 OD surface. Moving into the bulk of Ti6Al4V(E)-Q1, away from the deposition, a transitional region, also of dark discoloration, was observed with variable thickness, measuring approximately 50- to 100-μm in depth (as shown in Fig. 12c).

A gradient in discoloration existed at the transition region, as the extent of the dark shade decreased moving into the bulk. This gradient was where the microstructure consisted of a basketweave structure and further into the bulk, partial martensite was present. The same gradient was observed for the inner-sleeve OD surface of Ti6Al4V(F)-Q1. The region of discoloration, with a more distinct uniformity, extended approximately 50-μm into the bulk of Ti6Al4V(F)-Q1, after which, small grains of basketweave structure also transitioned into coarse-grained partial martensite.

Fig. 14 displays BSE images that clearly illustrate the morphological distinction of the deposition, α-case layer, and microstructural transition into the bulk. The equiaxed grains contained small, globular deposits arranged along grain boundaries. The α-case region contrasted greatly with the other areas in the image, exhibiting a smooth and porous texture. The pores (measuring 1.0- to 8.0-μm in diameter) of the α-case layer appeared to have a preferential arrangement near the interface between the α-case layer and transitional bulk region where the lamellar features of the Widmanstätten structure were present, with a layer of short, flake-like α that measured approximately 75-μm in thickness.

3.2.3. PLBD roller – bulk

Fig. 15 provides regions from which micrographs in Figs. 13 – 19 were obtained The partial martensitic bulk microstructure, observed beyond α-case layers for both Ti6Al4V sleeves in Q1, Fig. 13a-b, contained serrated α, which was resolved at higher magnification as shown in Fig. 13c. The martensitic structure gradually transitioned into acicular

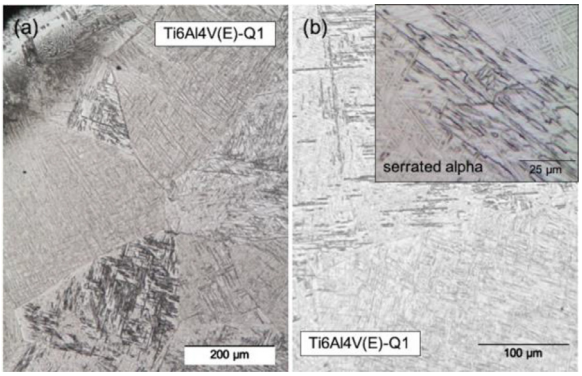

Fig. 13. Micrograph of Ti6Al4V(E)-Q1 in E1 region of bulk; (a) 100X, (b) 200X, (c) 500X; Kroll's.

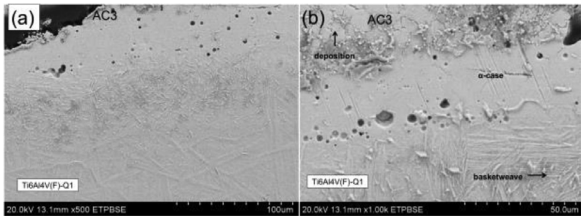

Fig. 14. (a)-(b) BSE micrograph of inner-sleeve OD edge surface of Ti6Al4V(F)-Q1 at (a) inner-sleeve spacing approximately 1-mm beyond notch region.

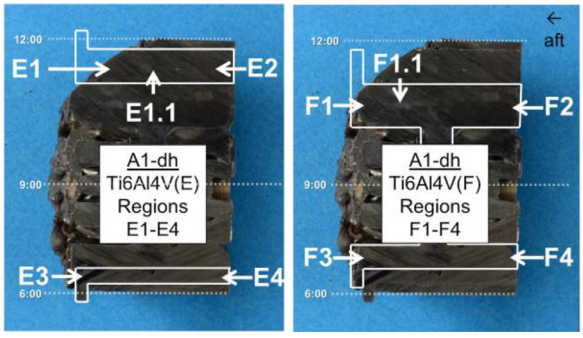

Fig. 15. Image of Sample A1-dh. Regions E1-E4 of Ti6Al4V(E) and F1-F4 of Ti6Al4V(F) labeled and outlined in white.

α in an aged transformed β matrix and at approximately 0.76-cm away from the reaction interface, Ti6Al4V(E) transformed into, and remained as, a bimodal structure of elongated primary α grains in a transformed β matrix (Fig. 16a). The matrix consisted of coarse, plate-like α and β, as shown in Fig. 16b-c. A bimodal microstructure is typically yielded from solution heat treating to 845–930 °C and subsequent aging below the β transus. As seen in Fig. 17, Ti6Al4V(E)-Q4 contains a bimodal microstructure comparable to that of Ti6Al4V(E)-Q1. The volume fraction of primary α is higher for Ti6Al4V(E)-Q4 than for Ti6Al4V(E)-Q1.

The volume fraction of primary α decreases slightly in Ti6Al4V(E)-Q4 moving away from the surface of the roller, which is typically attributed to decreased aging temperature or aging time. Presented in Fig. 18, the acicular α structure of Ti6Al4V(F) transitioned into, and remained as, a structure containing basket-weave acicular α (Widmanstätten) with prior β grain boundaries, the dark basketweave typical of an overaged β annealed structure 980 °C [4].

Similar to Q1, Fig. 19a-b shows the microstructure of Ti6Al4V(F)-Q4 to be partially martensitic near the surface and a gradient is also present in Ti6Al4V(F)-Q4 as the transition to large colonies of Widmanstätten α was observed and it was maintained for the remaining bulk, moving away from the reaction front, Fig. 19c-d. Ti6Al4V(F) was absent of the bimodal structure observed within Ti6Al4V(E).

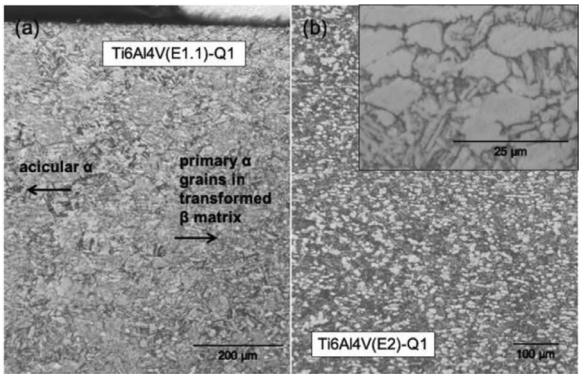

Fig. 16. Micrograph of Ti6Al4V(E)-Q1 in (a) E1.1 region, approximately 1.5-cm from the reaction front, 100X; (b) E2 region approximately 3.3-cm away from reaction front, 100X, and 100X; Kroll's.

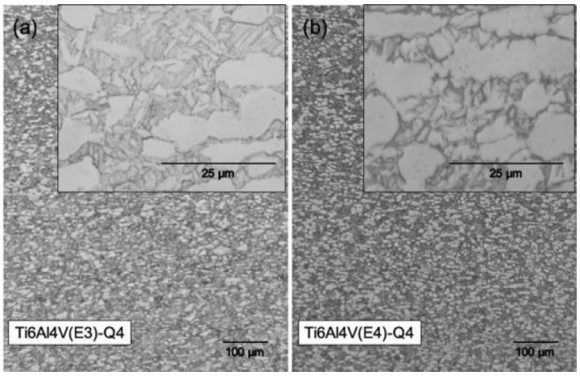

Fig. 17. Micrograph of Ti6Al4V(E)-Q4 in (a) E3 region of bulk at the reaction front, 100X and (b) 1000X; (c) E4 region of bulk approximately 3.3-cm away from reaction front, 100X and (d) 1000X; Kroll's.

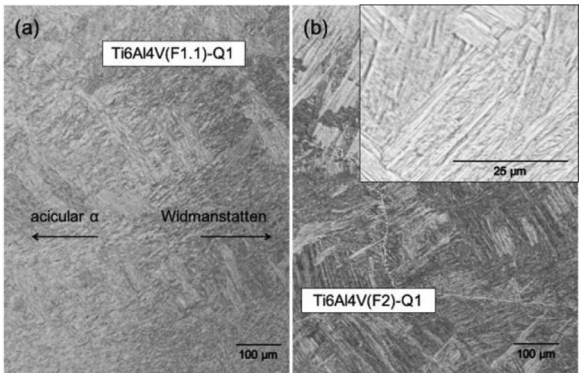

Fig. 18. Micrograph of Ti6Al4V(F)-Q1 in (a) F1.1 region, approximately 0.76-cm from the reaction front, 100X and in (b) F2 region of bulk approximately 3.3-cm away from reaction front, 100X and (c) 1000X; Kroll's.

3.3. Arc-jet specimens microstructural analysis

3.3.1. Arc-jet specimens – RSMM

On the surface of Class II and Class III samples, RSMM was observed and characterized by a globular, dendritic morphology. The RSMM shown in Fig. 20a-b, contained spherical and irregular pores of various sizes along with cracking and interdendritic voids. Void coalescence appeared to be the cause of the weak adherence seen in Fig. 20a where the

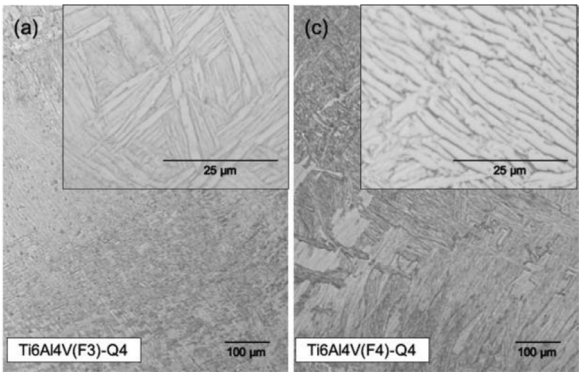

Fig. 19. Micrograph of Ti6Al4V(F)-Q4 in (a) F3 region of bulk at the reaction front, 100X and (b) 1000X; (c) F4 region of bulk approximately 3.3-cm away from reaction front, 100X and (d) 1000X; Kroll's.

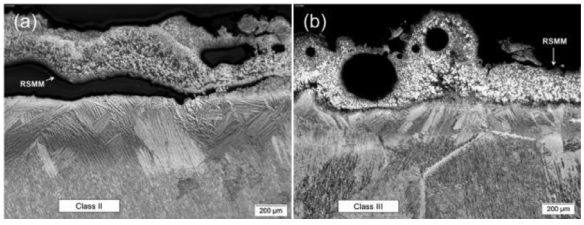

Fig. 20. Micrographs of (a) Class II and (b) Class III arc-jet samples, 50X; Kroll's.

RSMM is detached from the bulk surface. Beyond the RSMM, the edge bulk surface contained coarsened plate-like α. The region of coarsened plate-like α appeared lighter in color nearest to the surface and exhibited a basketweave morphology as it transitioned into large grains of acicular α and martensite.

3.3.2. Arc-jet specimens – alpha-case and oxides

The Class II α-case edge surface was rough and the α-case layer, also exhibiting a featureless full-α composition, similarly contained finger-like coarse plate-like α that transitions into a Widmanstätten structure. Moving into the bulk, the basketweave colonies transformed into a partial martensitic structure with a prior β grain boundary appearing as a boundary between the two morphologies. The α-case layer of Class III contained voids and longitudinal cracking along its length and the finger-like coarse α plates appeared more woven as it transitioned into a Widmanstätten structure, beyond which, partial to fully martensitic grains were apparent. Grain boundaries at the interface between Widmanstätten and the martensitic structure were distinct, appearing light in appearance with the enrichment of α phase.

3.3.3. Arc-jet specimens – bulk

Fig. 21 depicts the microstructural features of the arc-jet samples. The unaffected plate, Fig. 21a contained α and intergranular β. The grains are slightly elongated, likely the result of the working process. The unaffected plate structure serves as the representative original microstructure of the tested samples from Class I-III. Alpha-case is observed on the leading edge of the tested samples, Fig. 21b, it was observed that Class I had the thickest α-case layer compared to Class II and Class III. The α-case edge surface on the Class I sample was smooth and the α-case layer was relatively uniform and featureless with minor cracking apparent. The α-case layer transitioned into a coarsened plate morphology, that appeared as finger-like projections. The structure then transitioned into a Widmanstätten structure.

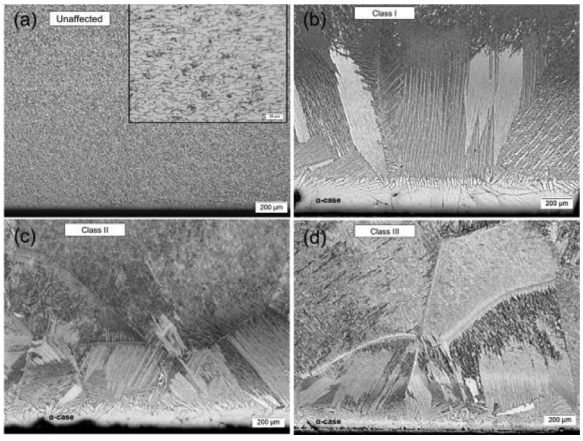

Fig. 21. Micrographs of arc-jet samples, (a) untested (b) Class I (c) Class II, (d) Class III, 50X; Kroll's.

4. Discussion

It can be well-reasoned that the oxygen-rich, superheated hypersonic flow conditions experienced by the orbiter during re-entry and subsequent vehicle breakup allowed for high-temperature oxidation to occur within various regimes. The globular oxide morphology and surface voids observed throughout the reaction front surface appear to be the result of oxygen dissolution at the surface. The spherical structures are likely hollow, and the pores may represent an interior look into the oxidation reaction products - the most notable surface pore containing a purple patina interior coating [5–7].

High temperature oxidation, a precursor to combustion, is further evidenced by the α-case formations observed along the reaction front surface. The oxygen enriched α-case develops simultaneously with the formation of the oxide layer as interstitial oxygen migration in this area stabilizes the α phase, leading to a brittle supersaturated α region, as well as increased hardness within and beyond the depth of the α-case layer. The α-case depth increases with thermal oxidation temperature and time, just as with the oxide layer [8], mainly following a parabolic relationship at 593 °C and 700 °C in Ti-6Al-4V [8]. The presence of multilayered α-case layers along the RSMM points to prolonged high-temperature oxidation occurring after the initial high-temperature excursion that caused melting. It also suggests the occurrence of subsequent deposition of melt over top molten material containing an already formed α-case layer.

The difference in α-case thickness observed along the titanium surfaces and the RSMM provides insight into the varying extent of oxidation along the surface and the dynamic break-up environment during the accident. With increasing temperatures, oxygen's diffusivity is increased, which serves as a possible explanation for the increased α-case thickness of the RSMM, as compared to the bulk surface. Increased hardness measurements obtained nearest to the reaction front is consistent with the α-case present in the region and the sustained hardness readings seen beyond the presence of α-case can be attributed to the martensitic microstructure and possible diffused oxygen [9]. Interstitial oxygen is a known strong α -phase stabilizer in Ti-6Al-4V and influences the martensitic transformation of β-phase to α'-phase [10]. The first observed hardness value, followed by a decrease in hardness, then subsequent high values, may be the result of multi-layered α-case formation within the RSMM.

For high-purity titanium alloys, serrated α is produced upon quenching from above the β transus. As the concentration of β-stabilizing elements increase, the transformation upon quenching results in acicular α [11]. The bimodal microstructure, consisting of slightly elongated primary α within transformed β, was concluded to be the initial microstructure of both titanium sleeves. Annealing to 650–815 °C,

results in the recrystallization of elongated structures, providing reasonable basis for the assumed initial condition. The microstructural gradient present within the microstructures suggests uneven transfer of heat within the roller components. Each component exhibited microstructural gradients at various depths moving away from the reaction front. The microstructures observed indicate a thermal gradient heating, where the reaction front experienced the highest temperatures, and moving away from the surface into the bulk, the temperature to which the roller was exposed decreased.

Heating to above the β transus 980 °C with subsequent fast cooling yields the martensitic microstructure that was observed beyond the α-case layers of the reaction front for both Ti6Al4V sleeves. The transition into a coarse, lamellar α structure, moving away from the reaction front, represents a slower cooling rate from above the β transus. Another transition occurs for Ti6Al4V(E) Q1, as acicular α transforms into a bimodal microstructure that is typical for Ti-6Al-4V when heated to temperatures below the β transus. The remaining bulk of Ti6Al4V(E)-Q1 consisted of this bimodal microstructure was assumed to represent the initial microstructure of Ti6Al4V(E). The Ti6Al4V(E)-Q4 microstructure did not transition into a bimodal morphology, but instead retained a lamellar structure that coarsened moving away from the reaction front. The Ti6Al4V(F) microstructure in the Q4 region closely mirrors that of the Q1 region with the same transition of martensite to acicular α occurring at a depth closer to the reaction front and no bimodal microstructure was present.

To the extent of the authors knowledge, Ti6Al4V(F) was not processed differently than Ti6Al4V(E) and the initial microstructure is the same for both Ti-6Al-4V sleeves. Therefore, it is implied that the initial bimodal microstructure of the Ti6Al4V(F) sleeve experienced a complete transformation during breakup due to bulk heating above the β transus. This is supported by observed deposition of RSMM along the reaction front surfaces of Ti6Al4V(F), suggesting intimate contact with, and heating of, Ti6Al4V(F) by the molten metal flow, then followed by slow cooling.

Although the re-entry conditions to which the PLBD rollers were exposed are not well defined, the arc-jet samples still serve as a baseline reference for ignition/combustion characteristics, given the known test parameters under which the samples reacted. Other possible factors that do not allow for a direct correlation to the arc-jet samples include titanium sleeve geometry, sleeve configuration with a multi-alloy construction, and unknown initial microstructural state or in-flight thermal history. The microstructure along the reaction front surface bore similarities to that of arc-jet samples, the greatest resemblance being to that of Class II and Class III specimens. Partial martensite was apparent within the bulk of the arc-jet samples and α-case formation along the reaction surface was present, along with the transitional region of plate-like α extending into the bulk. The RSMM of the arc-jet samples (although not incorporated with the melt of other alloy systems) was similar in that pores were present, representing oxygen dissolution. These observations, relating the microstructural features of Ti-6Al-4V within the PLBD roller to arc-jet samples, are in good agreement to the findings reported from a forensic study of thermally degraded Ti-6Al-4V X-links recovered from the *Columbia* accident [12].

5. Conclusions

An extensive characterization of a recovered PLBD latch roller from Space Shuttle *Columbia* was performed to evaluate material behavior during atmospheric re-entry of Ti-6Al-4V with an emphasis on the identification of ignition and/or combustion behavior. The nature of the damage observed on the roller provided an opportunity to compare features of heavily degraded region to regions that appeared nearly unaffected. It is understood by the authors that due to the complexity of the break-up environment conditions; conclusions must be drawn with caution.

Declaration of Competing Interest

The authors declare that they have no known competing financial interests or personal relationships that could have appeared to influence the work reported in this paper.

Acknowledgments

The authors would like to thank the following for their laboratory support: Christopher Bradley, Shalayna Smith and Brenda Machado of Herrera, Stafford and Associates. Columbia debris was made available for materials research through the *Columbia* Debris Loan Program.

This research did not receive any specific grant from funding agencies in the public, commercial, or not-for-profit sectors.

References

[1] J. Olivas, M. Wright, R. Christoffersen, D. Cone, S. McDaniels, Crystallographic oxide phase identification or char deposits obtained from space shuttle Columbia window debris, Acta Astronaut. 67 (2010) 553–560.
[2] National Aeronatics and Space AdministrationColumbia Crew Survival Investigation Report NASA/SP-2008-565, 2008.
[3] J. Olivas, B. Mayeaux, D. Cone, P. Melroy, W. Rochelle, Material Behavior of Titanium in Space Entry Environments, American Institute of Aeronautics and Astronautics (2011).
[4] ASM Handbook Committee, Atlas of microstructures IOF industrial alloys, in: T. Lyman (Ed.), Metals Handbook, 7, American Society for Metals, Metals Park, Ohio, 1972.
[5] M. Diamanti, B. Curto, M. Pedeferri, Interference colors of thin oxide layers on titanium, Color. Res. Appl. 33 (3) (2008) 221.
[6] D. Velten, V. Biehl, F. Aubertin, B. Valeske, W. Possart, J. Breme, Preparation of TiO_2 Layers on cp-Ti and Ti6Al4V by thermal and anodic oxidation and by sol-gel coating techniques and their characterization, J. Biomedic. Mater. Res. 59 (2002) 18–28.
[7] T.R. Strobridge, J.C. Moulder, A.F. Clark, Titanium Combustion in Turbine Engines FAA-RD-79-51, Federal Aviation Administration, Washington D.C, 1979.
[8] R. Gaddam, B. Sefer, R. Pederson, M.L. Antti, Study of alpha case depth in Ti-6Al-2Sn-4Zr-2Mo and Ti-6Al-4V, IOP Conference Series: Materials Science and Engineering, 2013.
[9] F. Pitt, M. Ramulu, Influence of grain size and microstructure on oxidation rates in titanium alloy Ti-6Al-4V under superplastic fomring conditions, J. Mater. Eng. Perform. 13 (6) (2004) 727–734.
[10] H. Miura, Y. Itoh, T. Ueamtsu, K. Sato, The influence of density and oxygen content on the mechanical properties of injection molded Ti-6Al-4V alloys, Adv. Powder. Metall. Part. Mater. 1 (2010) 46–53.
[11] F.H. Froes, Titanium: Physical Metallurgy, Processing, and Applications, 1st ed., ASM International, Materials Park, 2015.
[12] J. Buckner, S.W. Stafford, D.M. Cone, J. Olivas, Investigation of Ti-6Al-4V alloy response to atmospheric re-entry exposure, in: Proceedings of the 8th IAASS Conference in International Association for the Advancement of Space Safety, Melbourne, 2016.